



BNL-82253-2009-CP

Recent Results from the MINOS Experiment

Milind V. Diwan

Presented at the XIII International Workshop on Neutrino Telescopes
At the Istituto Veneto di Scienze, Lettere ed Arti, Venice, Italy
March 10-13, 2009

April 21, 2009

Physics Department
Electronic Detector Group
Brookhaven National Laboratory
P.O. Box 5000
Upton, NY 11973-5000
www.bnl.gov

Notice: This manuscript has been authored by employees of Brookhaven Science Associates, LLC under Contract No. DE-AC02-98CH10886 with the U.S. Department of Energy. The publisher by accepting the manuscript for publication acknowledges that the United States Government retains a non-exclusive, paid-up, irrevocable, world-wide license to publish or reproduce the published form of this manuscript, or allow others to do so, for United States Government purposes.

DISCLAIMER

This report was prepared as an account of work sponsored by an agency of the United States Government. Neither the United States Government nor any agency thereof, nor any of their employees, nor any of their contractors, subcontractors, or their employees, makes any warranty, express or implied, or assumes any legal liability or responsibility for the accuracy, completeness, or any third party's use or the results of such use of any information, apparatus, product, or process disclosed, or represents that its use would not infringe privately owned rights. Reference herein to any specific commercial product, process, or service by trade name, trademark, manufacturer, or otherwise, does not necessarily constitute or imply its endorsement, recommendation, or favoring by the United States Government or any agency thereof or its contractors or subcontractors. The views and opinions of authors expressed herein do not necessarily state or reflect those of the United States Government or any agency thereof.

Recent Results from the MINOS experiment

Milind V. Diwan

Physics Department, Brookhaven National Laboratory

Upton, NY 11973, USA

E-mail: diwan@bnl.gov

April 20, 2009

ABSTRACT

MINOS is an accelerator neutrino oscillation experiment at Fermilab. An intense high energy neutrino beam is produced at Fermilab and sent to a near detector on the Fermilab site and also to a 5 kTon far detector 735 km away in the Soudan mine in northern Minnesota. The experiment has now had several years of running with millions of events in the near detector and hundreds of events recorded in the far detector. I will report on the recent results from this experiment which include precise measurement of $|\Delta m_{32}^2|$, analysis of neutral current data to limit the component of sterile neutrinos, and the search for $\nu_\mu \rightarrow \nu_e$ conversion. The focus will be on the analysis of data for $\nu_\mu \rightarrow \nu_e$ conversion. Using data from an exposure of 3.14×10^{20} protons on target, we have selected electron type events in both the near and the far detector. The near detector is used to measure the background which is extrapolated to the far detector. We have found 35 events in the signal region with a background expectation of $27 \pm 5(stat) \pm 2(syst)$. Using this observation we set a 90% C.L. limit of $\sin^2 2\theta_{13} < 0.29$ for $\delta_{cp} = 0$ and normal mass hierarchy. Further analysis is under way to reduce backgrounds and improve sensitivity.

1. Introduction

In the current picture of neutrino oscillations, three flavors of neutrinos are related to three mass states by the Pontecorvo-Maki-Nakagawa-Sakata mixing matrix^{1,2)}. The mixing can be described by two Δm^2 parameters ($|\Delta m_{32}^2|$, $|\Delta m_{21}^2|$), three mixing angles (θ_{23} , θ_{12} , and θ_{13}) and a CP violating phase (δ_{cp})³⁾. The oscillation phenomena naturally falls into two domains: the atmospheric neutrino oscillations, and Solar neutrino oscillations³⁾. The atmospheric neutrino oscillations are well-described by $\nu_\mu \rightarrow \nu_\tau$ oscillations, with parameters $\sin^2 2\theta_{23} > 0.92$ and $1.9 \times 10^{-3} < |\Delta m_{32}^2| < 3.0 \times 10^{-3}$ eV² at 90% C.L.⁴⁾. The K2K experiment and MINOS have confirmed the atmospheric neutrino oscillations with accelerator beams^{5,6)}. Solar $\nu_e \rightarrow \nu_{\mu,\tau}$ oscillations are described by $\sin^2 2\theta_{12} = 0.86_{-0.04}^{+0.03}$ and $\Delta m_{21}^2 = 8.0_{-0.3}^{+0.4} \times 10^{-5}$ eV² are also consistent with multiple observations^{7,8)}, and are confirmed by disappearance of reactor $\bar{\nu}_e$ ⁹⁾. As yet, very little is known about either θ_{13} or δ_{cp} , although lack of observed disappearance of reactor $\bar{\nu}_e$ over a few km baseline¹⁰⁾ has shown that θ_{13} must be small: $\sin^2 2\theta_{13} < 0.19$ at 90% C.L. Furthermore, the sign of $|\Delta m_{32}^2|$ (or the ordering of the mass eigenstates) is unknown. The sign of Δm_{12}^2 is known using the strong matter effects that must be considered when analyzing neutrinos from the Sun. Determination of the unknowns in neutrino mixing needs further experiments

in the oscillation range of $|\Delta m_{32}^2|$ for conversion of muon and electron type neutrinos into each other.

For our present discussion, it is useful to exhibit an approximate analytic formula for the oscillation of $\nu_\mu \rightarrow \nu_e$ for 3-generation mixing obtained with the simplifying assumption of constant matter density^{11,12)}. Assuming a constant matter density, the oscillation of $\nu_\mu \rightarrow \nu_e$ in the Earth for 3-generation mixing is described approximately by Equation 1. In this equation $\alpha = \Delta m_{21}^2 / \Delta m_{31}^2$, $\Delta = \Delta m_{31}^2 L / 4E$, $\hat{A} = 2VE / \Delta m_{31}^2$, $V = \sqrt{2}G_F n_e$. n_e is the density of electrons in the Earth. Recall that $\Delta m_{31}^2 = \Delta m_{32}^2 + \Delta m_{21}^2$. Also notice that $\hat{A}\Delta$, which has absolute value of $LG_F n_e / \sqrt{2}$, is sensitive to the sign of Δm_{31}^2 .

$$\begin{aligned}
P(\nu_\mu \rightarrow \nu_e) \approx & \sin^2 \theta_{23} \frac{\sin^2 2\theta_{13}}{(\hat{A} - 1)^2} \sin^2((\hat{A} - 1)\Delta) \\
& + \alpha \frac{\sin \delta_{CP} \cos \theta_{13} \sin 2\theta_{12} \sin 2\theta_{13} \sin 2\theta_{23}}{\hat{A}(1 - \hat{A})} \sin(\Delta) \sin(\hat{A}\Delta) \sin((1 - \hat{A})\Delta) \\
& + \alpha \frac{\cos \delta_{CP} \cos \theta_{13} \sin 2\theta_{12} \sin 2\theta_{13} \sin 2\theta_{23}}{\hat{A}(1 - \hat{A})} \cos(\Delta) \sin(\hat{A}\Delta) \sin((1 - \hat{A})\Delta) \\
& + \alpha^2 \frac{\cos^2 \theta_{23} \sin^2 2\theta_{12}}{\hat{A}^2} \sin^2(\hat{A}\Delta)
\end{aligned} \tag{1}$$

For anti-neutrinos, the second term in Equation 1 has the opposite sign. It proportional to the CP violating quantity $\sin \delta_{CP}$. An accelerator experiment using high energy neutrinos, a sufficiently long baseline, and the ability to detect $\nu_\mu \rightarrow \nu_e$ conversion with low backgrounds and high statistics, has sensitivity to all four terms in Equation 1. The first term dominates the sensitivity to the unknown parameter θ_{13} . MINOS is the first high energy accelerator experiment so far to have sensitivity to more than the first term in Equation 1. In the following we describe an analysis of the MINOS data to reduce backgrounds to allow the observation of $\nu_\mu \rightarrow \nu_e$.

2. MINOS beam and detector

The MINOS detectors¹³⁾ and the NuMI beam line¹⁴⁾ are described elsewhere. In brief, NuMI is a conventional two-horn-focused neutrino beam with a 675 m long decay tunnel. The neutrino beam goes through the Earth to upper Minnesota over a distance of 735 km to the far detector. The horn current and position of the hadron production target relative to the horns can be configured to produce different ν_μ energy spectra. In figure 1 we show the spectrum of all ν_μ events in the fiducial volume for the horn-on and horn-off configurations. Several beam configurations with different mean energies have been used for studying backgrounds and systematics: in particular, the horn-off configuration has been particularly useful for the ν_e search.

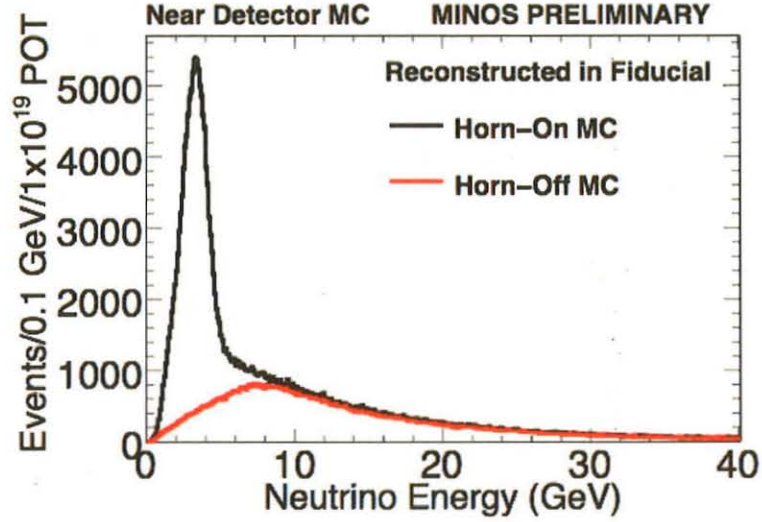


Figure 1: (in color) Spectrum of all muon neutrino events in the MINOS near detector fiducial volume for the horn on and horn off configurations.

The high energy, $\sim 5 - 10\text{GeV}$, obtained by moving the production target, as well as intermediate energy configurations have been used for the analysis of the beam systematics for the muon neutrino disappearance data. Most of the physics data has been in the low energy (horn-on) configuration in which the peak of the spectrum is $\sim 3\text{GeV}$. In the low energy configuration, 92.9% of the flux is ν_μ , 5.8% is $\bar{\nu}_\mu$ and 1.3% is the $\nu_e/\bar{\nu}_e$ contamination.

MINOS consists of two detectors: a 0.98 kt Near Detector (ND) 1.04 km from the NuMI target; and a 5.4 kt Far Detector (FD) 735 km from the target. Both are segmented, magnetized calorimeters that permit particle tracking, optimized for neutrino energy range of $1 < E_\nu < 50\text{GeV}$. The curvature of muons produced in $\nu_\mu + \text{Fe} \rightarrow \mu^- + X$ interactions^a is used for energy determination of muons that exit the detector and to distinguish the ν_μ component of the beam from the contamination. The energy of muons contained in the detector is measured by their range. The muon and shower energies are added to obtain the reconstructed muon neutrino energy ($E_{reco} = E_\mu + E_h$) with a resolution given by $\Delta p_\mu/p_\mu \approx 10\%$ and $\Delta E_h/E_h \approx 56\%/\sqrt{E_h}$. For electron neutrino detection the relevant parameters of the detector concern the calorimetric segmentation. Both the near and far detectors have identical segmentation of 1 inch (1.44 radiation length) steel and 1 cm thick plastic scintillator. Transversely the scintillator is in strips of 4.1 cm width, corresponding to Moliere radius of 3.7 for electromagnetic showers. The scintillator is read by wavelength shifting fibers into multianode PMTs. The scintillator strips range in

^aApproximately 5% of the neutrino interactions occur in aluminum and scintillator.

length from a maximum of 8 meters in the far detector down to ~ 1 m in the near detector. The light yield is on the average ~ 6 photo-electrons for a minimum ionizing particles. Although the near and far detectors have identical granularity, there are important differences: the light yield, the type of PMT used (Hamamtsu M16 in the far, and Hamamatsu M64 in the near), the cross talk between channels in the PMTs, and multiplexing of scintillator strips onto the PMT pixels¹³⁾. These differences are carefully calibrated using cosmic rays and simulated in the Monte Carlo programs to limit the near and far differences. After electron particle identification and selection cuts as described below, the energy resolution for ν_e events is $\sim 30\%/\sqrt{E}$.

3. Data Reduction

This note describes results from data recorded between May 2005, and July 2007. Over this period, a total of 3.36×10^{20} protons on target (POT) were accumulated. A 1.27×10^{20} POT subset of this exposure (hereafter referred to as Run I) forms the data set from Ref⁶⁾. In Run I and for most of the new running period (Run II), the beam line was configured to enhance ν_μ production with energies 1-5 GeV (the low-energy configuration). An exposure of 0.15×10^{20} POT was accumulated with the beam line configured to enhance the ν_μ energy spectrum at 5-10 GeV (the high-energy configuration). The Run II data were collected with a replacement target of identical construction due to failure of the motion system of the first target. The new target was found to be displaced longitudinally ~ 1 cm relative to the first target, resulting in a 30 MeV shift in the neutrino spectrum. This effect is incorporated in the Monte Carlo simulation, and the Run I and Run II data sets are analyzed separately to account for this shift.

The data reduction has several components: cuts are first applied to remove data from periods of bad detector and beam conditions. After event reconstruction, preselection cuts select events that are enriched in the types of events that are under analysis: negative or positive muons, electrons or neutral currents. These cuts are performed as identically as possible for the near and far detectors. Differences are accounted for in the Monte Carlo. After the preselection, particle identification cuts are applied to extract a pure sample of the events under consideration. The muon and neutral current analysis has been described in detail in previous publications^{15,16)}.

For the electron analysis the selected sample of data (the low energy horn on configuration) corresponds to 3.14×10^{20} protons on target for the far detector. The near detector data was sampled uniformly and scaled to correspond to 10^{19} protons on target. Reconstructed events were chosen within the well calibrated parts of the detectors corresponding to fiducial masses of 29 ton and 4 kton for the near and far detectors, respectively, within the 10 μ sec beam pulse gate to reject cosmic ray events. After these cuts cosmic contribute < 0.5 event background in the final sample. The ν_e preselection cuts selected an initial sample of events with single

electromagnetic showers according to the reconstruction algorithm and rejected events with any tracks longer than 25 planes. A second cut examined planes with track-like hits, and eliminated events with more than 16 planes with such hits. After the precuts, the event sample is composed of $\sim 30\%$ ν_μ CC events in which the muon is too short to be rejected, $\sim 65\%$ NC events, and about $\sim 5\%$ ν_e events from the beam contamination.

4. Selection of Electron Neutrinos

After preselection, further rejection of neutral current, and muon charged current events is needed. To achieve this rejection we use the short compact nature of the electromagnetic showers compared to the diffuse nature of hadronic showers. We have developed two software algorithms to examine each candidate event and classify it as a potential electron neutrino signal or background.

Selection ANN We use the pattern of energy deposition, after eliminating hits with less than 2 photo-electrons, to characterize each event by several parameters. The artificial neural network (ANN) algorithm combines 11 such reconstructed quantities that exhibit signal and background separation. Some of these quantities are the maximum energy fraction in 4 planes, fraction of energy in a 3 strip wide road, the RMS of transverse energy deposition, etc. The output from the ANN is between 0 (background like) and 1 (signal-like). With a cut at 0.7, the efficiency for the signal, after preselection, is expected to be approximately 41%; the expected neutral current and ν_μ CC rejection efficiency is $\sim 92.3\%$ and $\geq 99.4\%$, respectively.

Selection LEM The second discrimination technique is a novel approach called Library Event Matching (LEM) selection in which each event candidate is compared to a large library of simulated ν_e -CC and NC events. The best 50 library matches are found for each candidate event, by considering the probability that two different energy deposition patterns in the detector originated from the same neutrino interaction. This computationally intensive technique can be carried out because the size of the events is generally small, and all the strip information can be used. Three variables are constructed: the fraction of these matches that are ν_e -CC events, the mean hadronic y of the best matches, and the mean fractional charge q matched within those best matches. A likelihood is then formed from these variables as a function of energy. With a cut at 0.65, the efficiency for the signal, after preselection, is expected to be approximately 46%; the expected neutral current and ν_μ CC rejection efficiency is $\sim 92.9\%$ and $\geq 99.3\%$, respectively.

The two selection algorithms rely on very different techniques, provide different signal to background ratios, and are sensitive to different systematic uncertainties. Assuming the signal is at the Chooz limit, LEM has the potential to achieve a better signal to background ratio (1:3) compared to ANN (1:4), but it is more sensitive to systematic uncertainties on the relative energy calibrations in the near and far

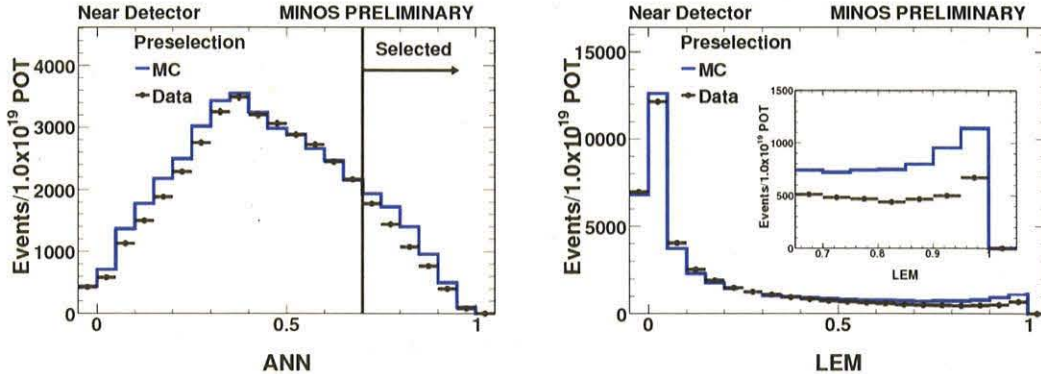


Figure 2: (in color) The ANN PID distribution for the near detector data (left). The LEM PID distribution for the near detector data (right). The plots show the chosen cuts for selection of ν_e -like events.

detectors. Both algorithms select predominantly NC events and higher y , ν_μ CC events. The background consists mainly of deep inelastic scattering events, with nearly half of the background showers containing a single π^0 . In the analysis reported here, the ANN selected sample is used to derive the final results, but the LEM selection is examined as a cross check.

5. Calculation of Backgrounds

The rate and spectrum of events selected as electron like in the near detector are used to predict the number of background events expected in the far detector. Figure 2 shows the distribution of ANN PID and LEM PID for the near detector data. The plots also show the prediction from the Monte Carlo which deviates from the data. This level of deviation is within the systematic errors due to cross section and hadronic shower modeling uncertainties. The Monte Carlo is based on past data¹⁷⁾ with much lower statistics in the MINOS energy region, and therefore while the Monte Carlo can be used for understanding ratios, and relative changes, the MINOS near data itself must be used to determine the normalization of the background in the far detector.

The near detector background spectrum has three different components, NC events, ν_μ -CC events and beam ν_e events. At lowest order the far detector background calculation is the near detector event rate (5524 events per 10^{19} POT for ANN) multiplied by the energy averaged far/near ratio of the neutrino flux $\sim 1.3 \times 10^{-6}$ and the ratio of the fiducial masses 4kton/29ton. However, the ν_μ charged current component of the background is affected by oscillations, and therefore a more sophisticated calculation is needed. For such a calculation we need to separate the background components and extrapolate them separately to the far detector. The far detector

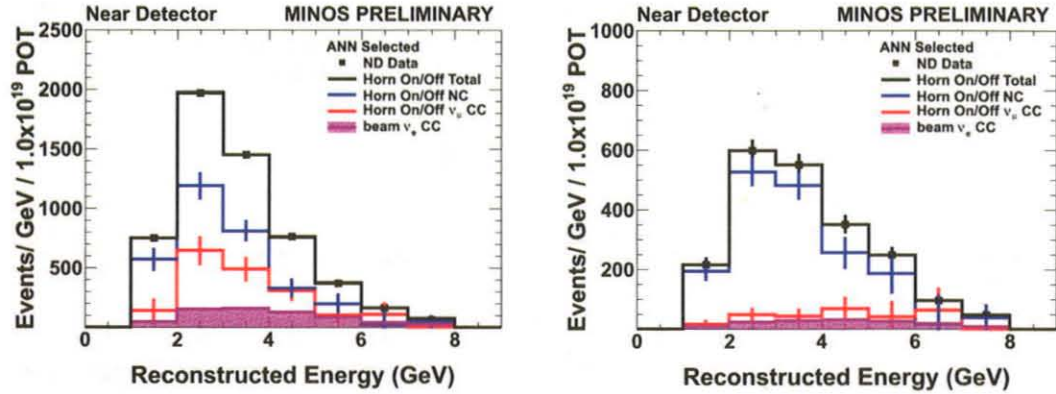


Figure 3: (in color) Separation of the types of backgrounds in the near detector data. A calculation is performed using the horn-off data which is enriched in NC events because of the higher energy neutrino spectrum (see text). Large fraction of the error is due to the statistics of the horn-off sample. This is for the ANN selection, results are similar for the alternate selection (LEM).

will also have a small component from ν_τ events which will be calculated by Monte Carlo.

The components of the background are determined using the horn off data sample recorded in the ND. Applying the ν_e selection to data taken with the focusing horns turned off (horn-off) provides a neutral current enriched sample. The higher mean energy spectrum (see figure 1) of the horn-off sample allows almost complete rejection of the ν_μ charged current events because the muons tend to be longer. These data are used in conjunction with the standard low energy beam configuration data (horn-on) to extract the individual NC and CC- ν_μ components of the samples as a function of reconstructed energy. The Monte Carlo is used to calculate the ratios r_{NC} and r_{CC} , which are the ratios of the horn-off to horn-on configurations for NC or CC events, respectively. An additional input from the Monte Carlo is the small contamination of ν_e events in the beam. With this information a calculation is performed for every energy bin to extract the CC and NC composition in both horn on and horn off spectra. Figure 3 shows the final result for the ANN selection. Integrating over the energy spectrum, the ND background is $57 \pm 5\%$ NC, $32 \pm 7\%$ ν_μ -CC and $11 \pm 3\%$ intrinsic beam ν_e -CC events. The errors on the NC and ν_μ -CC components arise from the statistics of the horn-off data and systematics on the ratios; the uncertainty on the beam ν_e -CC includes systematic errors from the beam flux, cross-section and selection efficiency for electrons.

After decomposing the Near Detector energy spectrum into its background components, each background spectrum is multiplied by the ratio of the Far to Near ratio from the MC simulation for each component to provide a prediction of the FD spectrum for that component. The far/near ratios are shown in figure 4 for the ANN selection. The MC simulations take into account differences in the spectrum of events

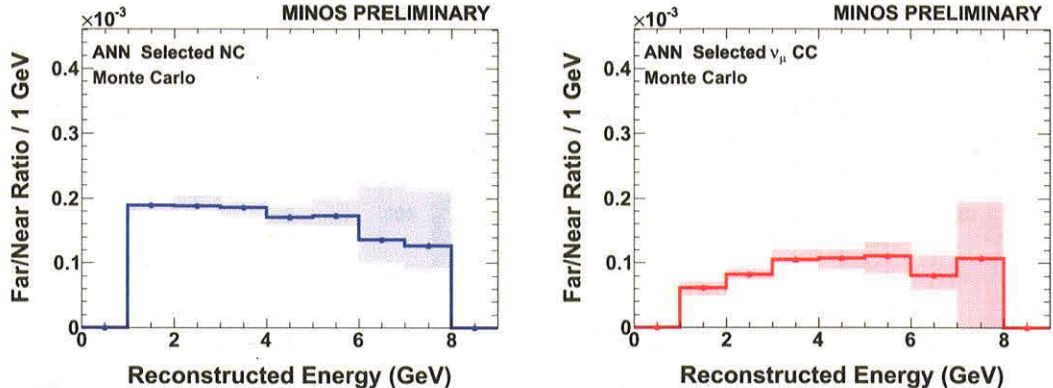


Figure 4: (in color) Monte Carlo calculation of the far/near ratios for NC and CC background components. The calculation includes effects of beamline geometry (including the $1/r^2$ loss), fiducial mass, difference in spectra, detector calibrations, and differences in the analysis efficiencies. Plots are similar for the alternate selection (LEM).

at the ND and FD due to the beam line geometry as well as possible differences in detector calibrations and topological response. Oscillations are included when predicting the ν_μ -CC component. The smaller ν_τ -CC and beam ν_e -CC components are calculated by Monte Carlo using the expected energy spectrum in the FD. All background components are then added together and summed over the energy range to provide the total predicted background in the Far Detector. The detailed modeling of all far/near differences change the background prediction from the lowest order by $\sim 10\%$. We expect a total background of 26.6 events for the ANN selection, of which 18.2 are NC, 5.1 are ν_μ -CC, 2.2 are beam ν_e and 1.1 are ν_τ for 3.14×10^{20} POT^b. With LEM, we expect 21.4 background events, with 14.8 NC, 2.9 ν_μ -CC, 1.1 beam ν_e and 2.7 ν_τ .

The effects of systematic errors were evaluated by generating modified MC samples, and quantifying the change in the number of predicted background events in the Far Detector using Far to Near ratios from the modified samples relative to the unmodified case. Many uncertainties, including those that affect neutrino interaction physics, shower hadronization, intranuclear re-scattering, and absolute energy scale errors affect the events in both detectors in a similar manner and largely cancel. Other effects give rise to Far/Near differences such as relative event rate normalization, calibration errors, reconstruction differences between the detectors and low level modeling of each detector. The individual systematic errors are added in quadrature along with the systematic error arising from the decomposition of the background sources in the ND to give an overall systematic error of 7.3% on the number of background events selected with the ANN selection. The LEM selection is more sensitive

^bUsing $\Delta m_{32}^2 = 2.43 \times 10^{-3} \text{eV}^2$, $\sin^2 2\theta_{23} = 1.0$, and $\sin^2 2\theta_{13} = 0$.

to uncertainties in the PMT gains, relative energy calibration and crosstalk. The total systematic error on the number of background events selected by the LEM technique is 12.0%.

5.1. Examination of events outside the signal region and other checks

Three main checks are performed by utilizing an independent data set obtained from ν_μ charged current events in which the muon is removed in software and the remaining hadronic shower is analyzed as if it is a complete neutrino event. This procedure is carried out on data and MC and the ν_e selections are applied to both. The discrepancy between muon-removed data and MC simulation is similar to that found in the standard sample as a function of reconstructed energy and of many different reconstructed shower topology variables used in the selections.

In the first check, the muon-removed data is used to obtain the relative contributions of the background components present in the ND data spectrum. The number of selected NC events in the MC simulation of the standard sample is scaled in each energy bin by the ratio of the number of events in the muon-removed data to the muon-removed simulation. Once the number of NC events is determined, the number of ν_μ -CC events selected in each reconstructed energy bin in the data is determined using $N_{CC} = N_{total}^{data} - N_{NC} - N_{\nu_e}$, in which the number of beam ν_e events are obtained from the MC. The background components as derived from the muon-removed sample agree well with those obtained from the horn-off method.

In the second check, we treat the muon removed data from the near and far detectors as if they are real events and perform a complete analysis. From the near data we create a prediction for the far detector and count the number in the far detector. Using this procedure we predicted $29 \pm 5(stat) \pm 2(syst)$ events for the ANN selection and observed 39 events. For the LEM selection the prediction was $17 \pm 4(stat) \pm 2(stat)$ and the observation was 25. The observed excess in this sample, which contains no electron signal events, was a cause of concern, however, upon examination of the full distribution with and without the particle ID cut, it was considered likely to be a statistical fluctuation. This issue will be explored with the larger data sample being acquired at this time.

In the third check, we estimate the efficiency for selecting ν_e -CC events. We use the sample of muon removed events and embed a simulated electron of the same momentum as the removed muon. Test beam measurements indicate that electrons are well simulated in the MINOS detectors. Data from the test beam ¹⁸⁾ was analyzed using the same selection cuts and agrees with Monte Carlo within 2.6% for ANN and 2.2% for LEM. sxs Comparisons between muon-removed data and simulated samples of events with embedded electrons indicate that the selection efficiency of ν_e signal events is well modeled by the MC. The algorithms focus on the EM core of the shower and are not affected by hadronic shower modeling discrepancies. The

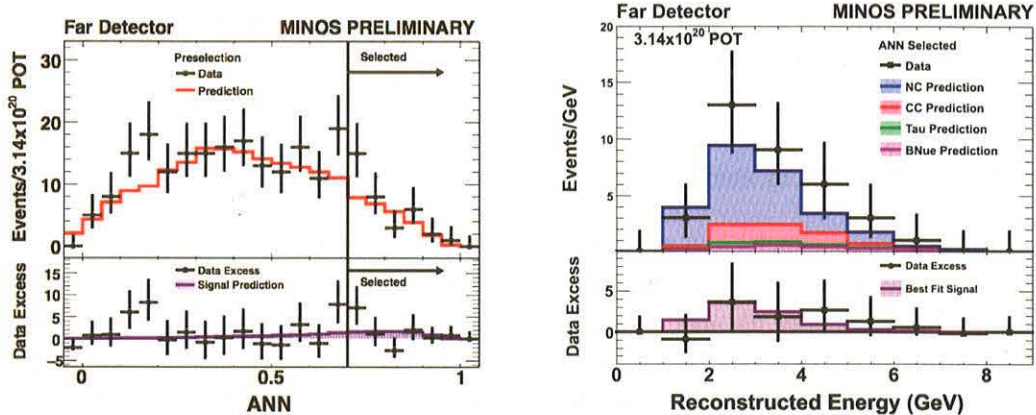


Figure 5: (in color) Distribution of far detector events for the ANN PID. Left shows the ANN PID distribution. Right shows the energy distribution after the PID cut. The plots below show the data minus the background prediction with the expected distribution of the signal if all the excess is interpreted as signal.

difference between the data and the MC is used as a correction to the signal selection efficiency and it is -0.3% for ANN and -5.3% for LEM. The selection efficiency of the ANN selection is calculated to be $41.4 \pm 1.4\%$ and for LEM is $45.2 \pm 1.5\%$.

The prediction of the backgrounds in the FD and the systematic uncertainties on that prediction were established before examining the data in the FD. Some additional checks were performed before opening the signal region. The number of events passing the preselection cuts, but failing the ν_e -CC selection cuts were compared to the expectation. In the FD data, 146 events were observed below the ANN selection cut, with an expectation of $132 \pm 12(\text{stat}) \pm 8(\text{syst})$. The events below the LEM cut totaled 176 events compared to an expectation of $157 \pm 13(\text{stat}) \pm 3(\text{syst})$. Both observations deviate from the background prediction by approximately 1σ assuming no signal events in this part of the data.

6. Results for $\nu_\mu \rightarrow \nu_e$

After examining the sideband data sets, we proceeded to count the number of events passing the predetermined selection cut. We observe 35 events in the FD when using the ν_e selection based on the ANN algorithm, with a background expectation of $27 \pm 5(\text{stat.}) \pm 2(\text{syst.})$. With LEM (the secondary selection) we observe 28, with a background expectation of $22 \pm 5(\text{stat.}) \pm 3(\text{syst.})$. The distributions are shown in Fig. 5 and 6.

Figure 7 shows the 90% confidence level interval in the $\sin^2 2\theta_{13}$ and δ_{CP} plane for each mass hierarchy using our observation for ANN PID. To set this limit we have used only the total observed number of events; detailed fitting of the data distributions was not performed for this result. We use the current best fit value of

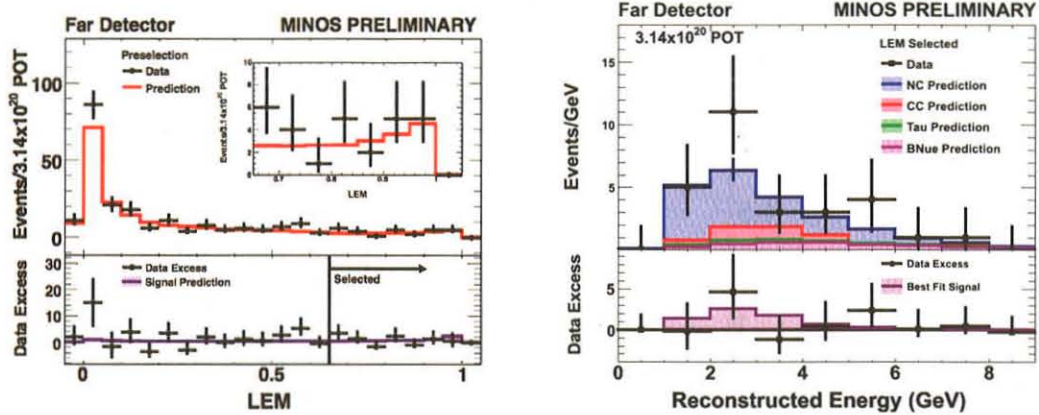


Figure 6: (in color) Distribution of far detector events for the LEM PID. Left shows the LEM PID distribution. Right shows the energy distribution after the PID cut. The plots below show the data minus the background prediction with the expected distribution of the signal if all the excess is interpreted as signal.

$|\Delta m_{32}^2| = 2.43 \times 10^{-3} \text{ eV}^2$ and $\sin^2(2\theta_{23}) = 1.0$ for this calculation. Fluctuations (Poisson) and systematic effects (Gaussian) are incorporated via the Feldman-Cousins approach³⁾. The oscillation probability is computed using a full 3-flavor neutrino mixing framework that includes matter effects.

7. Updates to MINOS measurement of ν_μ disappearance

MINOS has recently reported updated measurements of ν_μ disappearance¹⁹⁾ on the same data set that was described above (the high energy spectrum data was also included). We observed 848 ν_μ -CC events in the far detector across the energy range of 0 to 120 GeV compared to the expectation of 1065 ± 60 (*syst*). The observed spectrum is shown in figure 8. The same figure also shows the confidence interval in the $\sin^2 2\theta_{23}$ versus $|\Delta m_{32}^2|$ plane. We obtain $|\Delta m_{32}^2| = 2.43 \pm 0.13 \times 10^{-3} \text{ eV}^2$ at 68 % C.L. and the mixing angle of $\sin^2 2\theta_{23} > 0.90$ at 90% C.L. At present time the measurement of $|\Delta m_{32}^2|$ is dominated by MINOS and the measurement of the mixing angle is dominated by Super-Kamiokande.

While the disappearance of ν_μ from the atmosphere and the NuMI/MINOS beam experiment is largely explained by 3 generation neutrino mixing with $\nu_\mu \rightarrow \nu_\tau$ as the mechanism, any small admixture of sterile neutrinos is still an experimental issue. MINOS performed a search for disappearance of active neutrinos using neutral current interactions¹⁶⁾. The final spectrum of neutral current events and the prediction based on near detector data is shown in figure 9. No anomalous depletion in the reconstructed energy spectrum is observed. Assuming oscillations occur at a single mass-squared splitting, a fit to the neutral- and charged-current energy spectra limits the fraction of ν_μ oscillating to a sterile neutrino to be below 0.68 at 90% confidence

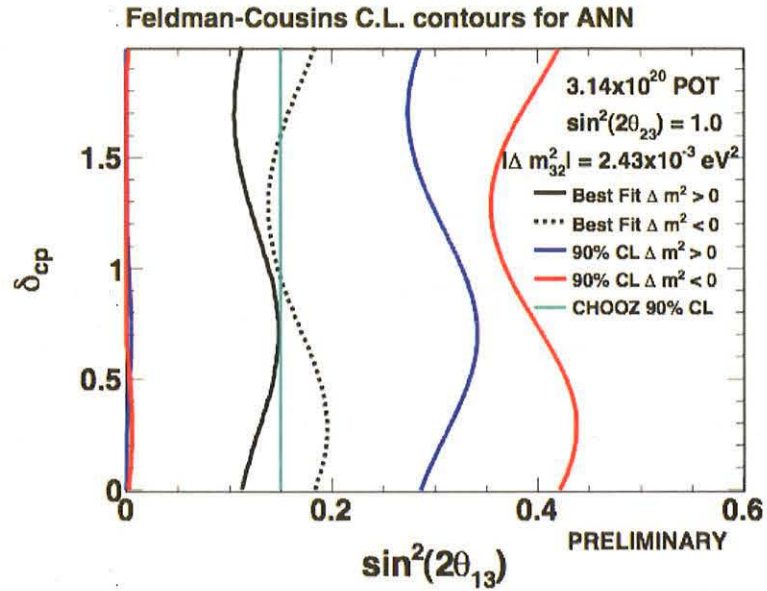


Figure 7: The 90% confidence interval in the $\sin^2(2\theta_{13})$ and δ_{CP} plane using the ANN PID results. Black lines show the best fit to our data in both the normal hierarchy (solid) and inverted hierarchy (dotted). Blue (red) lines show the 90 C.L. boundaries for the normal (inverted) hierarchy.

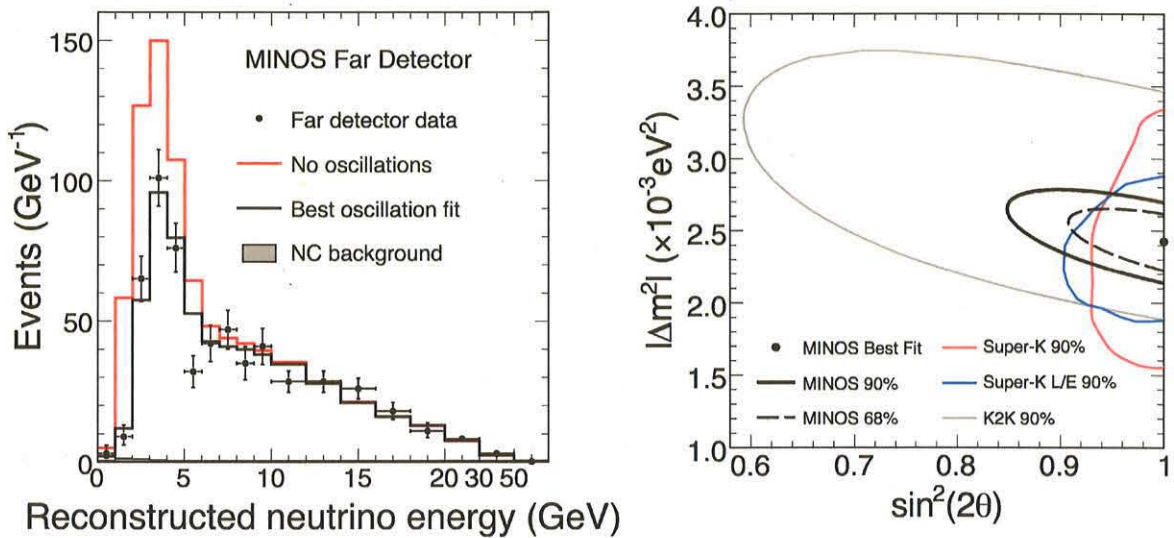


Figure 8: (in color) Measurement of MINOS for the disappearance of muon neutrinos.

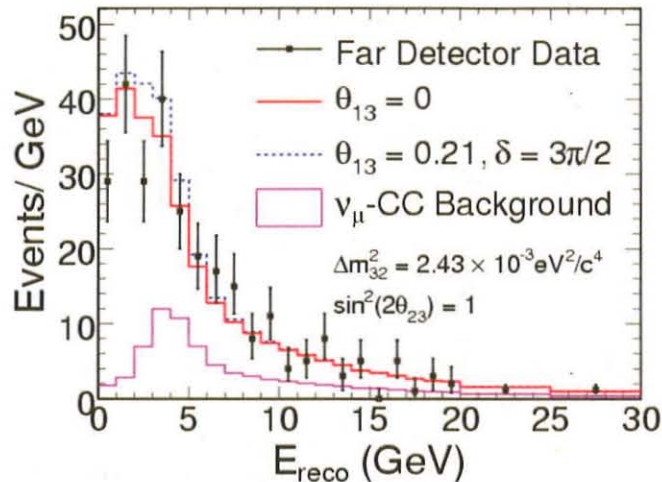


Figure 9: (in color) Measurement of Neutral Current spectrum in MINOS.

level. Electron neutrinos can constitute a background to the neutral current analysis, therefore any possible contribution from ν_e appearance at the current experimental bound leads to a less stringent limit.

8. Conclusions

In summary, we report the first results of a search for ν_e appearance in the MINOS experiment. The observed rate of events in the Far Detector after ν_e selection for 3.14×10^{20} POT is consistent with the background expectation within 1.5 standard deviations. For this data set, assuming $|\Delta m_{32}^2| = 2.43 \times 10^{-3} \text{ eV}^2$, $\sin^2(2\theta_{23}) = 1.0$, and $\delta_{CP} = 0$, we set an upper limit of $\sin^2(2\theta_{13}) < 0.29$ at 90% C.L. for the normal hierarchy and $\sin^2(2\theta_{13}) < 0.42$ for the inverted hierarchy.

9. Acknowledgements

This was prepared for the proceedings of the XIII International Workshop on Neutrino Telescopes at the Istituto Veneto di Scienze, Lettere ed Arti in Venice held on March 10-13, 2009. The presentation was on behalf of the MINOS collaboration. This work was supported by the US Department of Energy under contract number DE-AC02-98CH10886.

10. References

- 1) B. Pontecorvo, JETP 34, 172 (1958).
- 2) Z. Maki, M. Nakagawa, and S. Sakata, Prog. Theor. Phys. 28, 870 (1962).

- 3) W.M. Yao *et al.*, J. Phys. G 33, 1 (2006).
- 4) Y. Ashie *et al.*, Phys. Rev. Lett. 93, 101801 (2004); Phys. Rev. D71, 11 2005 (2005).
- 5) M.H. Ahn *et al.*, Phys Rev D 74 072003 (2006).
- 6) D.G. Michael *et al.*, Phys. Rev. Lett. 97, 191801 (2006);
- 7) J. Hosaka *et al.*, Phys. Rev. D73, 112001 (2006).
- 8) S.N. Ahmed *et al.*, Phys. Rev. Lett. 92, 181301 (2004).
- 9) T. Araki *et al.*, Phys. Rev. Lett. 94, 081801 (2005).
- 10) M. Apollonio *et al.*, Eur. Phys. J., C27, (2003)331.
- 11) M. Freund, Phys.Rev. D64 (2001) 053003; M. Freund, P. Huber, M. Lindner, Nucl.Phys. B615 (2001) 331-357;
- 12) A. Cervera, *et al.*, Nucl. Phys. B579(2000) 17.
- 13) D.G. Michael *et al.*, Nucl. Instrum. Meth. A596:190-228, 2008
- 14) S. Kopp, Proc. 2005 IEEE Part. Accel. Conf., May 2005, Fermilab-Conf-05-093-AD and arXiv:physics/0508001.
- 15) P. Adamson *et al.*, Phys. Rev. D77, 072002 (2008).
- 16) P. Adamson *et al.*, Phys. Rev. Lett 101: 221804, 2008.
- 17) H. Gallagher, Nucl. Phys. B (Proc. Suppl.) 112, 188 (2002); update at arXiv:0806.2119 (2008).
- 18) P. Adamson *et al.*, Nucl. Inst. & Meth. A556, 119 (2006).
- 19) P. Adamson *et al.*, Phys. Rev. Lett 101, 131802, 2008.